Variable Speed Control in PATs: Theoretical, Experimental and Numerical Modelling

Frank A. Plua [1,2], Francisco-Javier Sánchez-Romero [3], Victor Hidalgo [4], Petra Amparo López-Jiménez [1] and Modesto Pérez-Sánchez [1,*]

1   Hydraulic and Enviromental Engineering Department, Universitat Politècnica de València, 46022 Valencia, Spain; fapluagu@doctor.upv.es (F.A.P.); palopez@upv.es (P.A.L.-J.)
2   Carrera de Ingeniería Civil, Facultad de Ingeniería y Ciencias Aplicadas, Universidad Central del Ecuador, Quito 170129, Ecuador
3   Rural and Agrifood Engineering Department, Universitat Politècnica de València, 46022 Valencia, Spain; fcosanro@agf.upv.es
4   Centro de Investigación en Mecatrónica y Sistemas Interactivos—MIST, Universidad Indoamérica, Av. Machala y Sabanilla, Quito 170103, Ecuador; vhhidalgo@uce.edu.ec
*   Correspondence: mopesan1@upv.es

Abstract: The selection of pumps as turbines (PATs) for their respective use in energy optimisation systems is a complicated task, because manufacturers do not provide the characteristic curves. For this reason, some research has been carried out to predict them with computational fluid dynamics (CFD) and mathematical models. The purpose of this study is to validate these two prediction methodologies of flow (Q) vs. head (H) curves through numerical modelling using the computational package OpenFOAM, together with a comparison with the experimental data obtained from a PAT for the case in which the nominal rotation speed of the machine varies. Depending on the configuration and working conditions of the PAT, the simulation performed with OpenFOAM was validated by calibrating it with the nominal curve of the pump and with another simulation performed with CFD workbench SOLIDWORKS FloEFD. Subsequently, the second methodology related to the analyses and mathematical models proposed to predict the Q vs. H curves were also validated with new models in OpenFOAM and the experimental data. The results show that these prediction methods are effective when a machine's operating point is close to the BEP (best efficient point). The absolute error ranges obtained with these two prediction methodologies for rotation speeds of 880 rpm, 1020 rpm, 1200 rpm, and 1500 rpm are between 5 and 24%, 2 and 17%, 0 and 12%, and 1 and 24%, respectively.

Keywords: pumps as turbines (PAT); computational fluid dynamics; variable rotational nominal speed; OpenFOAM

1. Introduction

The availability of water resources at the global level has significantly decreased. Among the main agents that have caused this situation are climate change, environmental pollution, human activities, and failures in hydraulic structures, among others. It is becoming increasingly complicated to access appropriate sources that meet the quality and quantity of the resource. Despite this, water loss due to leaks in pressurised distribution systems still manages considerable values, with losses of 8 to 24% in developed countries [1]. Considering that the need for water is increasing, there is an urgent need to implement sustainable projects that allow the user to carry them out efficiently [2]. This type of project requires the use and development of new technologies that are easy to implement and apply [3].

In the case of sustainable water systems, there are some approaches from which improvements can be proposed. Among these approaches are the determination of water

quality parameters [4], optimisation of energy efficiency [5,6] reduction of water leaks [7,8], mathematical modelling of management, and optimisation of systems [9,10], among others.

Water distribution systems are not energy-efficient, because they depend on pressure demands that can generate leaks, increasing energy costs [11]. One of the elements that has a negative effect from the point of view of energy efficiency but is necessary for the hydraulic operation of systems is the pressure-reducing valve (PRV) [12]. PRVs are used to reduce the pressure at one point by regulating the flow passage. An alternative to the use of these devices, to reduce the dependence on non-renewable energy [13] and take advantage of the excess energy of these systems [14], is the use of PATs (pumps working as turbines). In addition, PATs have been used as energy-generating devices in micro-hydroelectric power plants as a sustainable solution in the water industry [15]. For this reason, it has become a trend to study the use of PATs to optimise different water systems to improve their sustainability [16–18].

PATs are pumps that work in reverse mode to generate energy. This machine's cost is cheaper than a conventional turbine of the same size [19], although they have lower hydraulic efficiencies in ranges between 0.6 and 0.7 [20]. When all electromechanical equipment is considered, the overall efficiency decreases to values between 0.5 to 0.6 [21]. The use of pumps operating as turbines (PATs) has increased due to their application, availability, and cost advantages [6,22–27]. For example, Novara et al. [28] concluded that an installation with PATs could be 5 to 15 times cheaper than a conventional installation with turbines.

The study of PATs began with Thoma and Kittredge [29], who accidentally found that pumps can operate efficiently as turbines when trying to evaluate the complete characteristics of pumps. In 1957, Stepanoff [30] reported several modes of operation of the pumps on performance curves plotted in quadrants. Once it was discovered that PATs could be applied in the chemical industry and the supply of drinking water, different researchers developed some techniques to predict the operation of this type of machine. In 1962, Childs [31] carried out comparative studies between efficiencies in devices working in both modes (pump–turbine). Subsequently, the first studies were carried out to predict the performance values in turbine mode and discover the best efficient point (BEP) through linear equations. The study of PATs has been developed using different approaches, such as in water distribution systems, where Jain [32] researched placing PATs in distribution systems. Fecarotta [33] and Morani [11] proposed an analysis regarding the proper location of PATs; the latter focused the research to look for cost reduction and the maximisation of production and energy savings. Moazeni [34] investigated the optimal number and location of PATs through mixed nonlinear programming models. Macias [18] established a methodology that was applied in an irrigation project in a rural area in the province of Valencia (Spain) that focused on optimising the location and selection of PATs based on the influence of leaks. The same author [13] developed a new methodology for self-calibration of leaks to learn the injected flow rate and the volume consumed in water networks. This methodology was applied in the city of Manta, Ecuador.

Since the performance curves are not available in pumps that work in turbine mode [27], different studies and methodologies have been carried out to obtain them and to select the appropriate machine depending on the type of working conditions required. Rossi [35] proposed a general method to predict PAT performance using artificial neural networks (ANN). Based on the datasheets provided by the pump manufacturers, the author obtained the BEP and off-design performance using the ANN methodology. In addition, the resulting predictions were compared with experimental data not used in the training process, which resulted in a high degree of compatibility. The study concluded that the BEP flow rate increased in reverse mode while the specific speed in BEP decreased slightly and also recommended the use of this tool to choose the proper PAT. To estimate the BEP and the characteristic curves of PATs, Perez-Sánchez [20] proposed new approach equations from an experimental base of 181 machines. Additionally, Plua [21] presented new empirical expressions to estimate the head, efficiency, and power curves for PATs with variable

speeds. These equations allow the application of various operation strategies in hydraulic simulation tools (e.g., Epanet and WaterGEMS).

Micro-hydroelectric power plants (MHP) have become very effective solutions for rural sectors with powers of 5–100 kW. The big problem with these facilities is the high turbine cost concerning the entire project [27]. In the case of MHP, the price of these elements can be higher than 60–70% [36]. One possibility to reduce this cost is to use PATs instead of a conventional turbine [37], which would favour the expansion of MHP and the reduction of greenhouse gas emissions [28]. In 2012, Pascoa [38] proposed a new approach for a hydroelectric plant with PAT with a constant flow. Rossi [39] suggested the economic feasibility of placing PATs in the Merano aqueduct, which resulted in the production of 338 kWh of daily electricity and power of 19.18 kW. Table 1 [27] shows different PAT installations in power generation projects.

Table 1. PAT installations in MHP [27].

Location	The Capacity of the Plant (kW)	Year of Installation
Sainyabulli Province, Laos	2	2008
Thima, Kenya	2.2	2001
Mae Wei Village, Thailand	3	2008
West Java, Indonesia	4.5	1992
Kinko village, Tanzania	10	2006
Fazenda Boa Esperanca, Brazil	45	2007
Ambotia Micro-hydro project, India	50	2004
British Columbia, Canada	200	-
Vysni Lhoty, Czech Republic	332	2008

CFD techniques have been widely used to predict characteristic curves and the performance of pumps in direct and reverse modes and proven to be an effective solution in PAT approaches [40–43]. Additionally, an experimental investigation is fundamental for obtaining reliable results for PATs under different optimisation stages [14,21,44,45]. Different types of machines, such as axial, mixed, and radial PATs with horizontal and vertical axes that single- and multistage [46], have been studied using CFD simulations for fixed and variable speeds [24–26]. However, very few studies related to numerical modelling in PATs of variable rotational speeds have been executed, so it is imperative to establish equations and laws that predict their behaviour [47]. The numerical simulations were carried out to define the performance of the pump [48], analyse the flow in turbine mode [49], predict and extrapolate the characteristic curves [50], etc.

Plua [40] presented research in which the main parameters and techniques that have been simulated for PATs through CFD are shown and which main simulation ranges are mentioned: specific speed: 0.8–306, rotational speed: 250–3900 rpm, flow rate: 2.9–300 L/s, and mass flow: 13–17.8 kg/s. Concerning the numerical simulations, the principal turbulence models used were Reynolds Average Navier–Stokes (RANS) and Unsteady Reynolds Average Navier–Stokes (URANS). The most used closure model was k-ε, followed by k-ω and k-ω-SST, among others. Regarding packages, ANSYS-CFX was the most used, followed by CFD Code Fluent and OpenFOAM. With respect to the mesh generation, the number of cells was 1×10^6 to 4.2×10^6, with hexahedral, tetrahedral, mixed blocks, and pyramids. Depending on each situation, boundary conditions such as the total pressure, mass flow rate, stagnation pressure, constant total pressure, static pressure, and volumetric flow were placed at the inlet and outlet of the model. In conclusion, it was established that the CFD methodology to predict the performance of a pump working as a turbine presented adequate accuracy based on the comparison of the results with the experimental tests. However, numerous errors were also reported in some studies. The authors assumed that the reported errors were due to the geometries between the tests and the simulations

not being identical; the loss estimation was not exact, and more experience in computational analysis is required for modelling this type of phenomenon. Finally, the same author [47] evaluated the application of numerical CFD simulation in PATs in comparison with experimental results and obtained conclusions for future numerical analyses. As a result, it was evidenced that there have been a few simulated cases where a flow with variable speed was simulated and that the number of studies with free code computational packages is minimal, and their use should be promoted due to their outstanding capabilities.

Therefore, the present study is focused on a numerical simulation in the OpenFOAM 3D free code package of PATs that have experimental data to validate the use of the new empirical expressions proposed for machines with different rotational speeds. The particularity in the modelling is that the study of a rotating PAT at different speeds will be carried out, and comparisons will be made with the experimental results obtained on a test bench to calibrate the model.

2. Materials and Methods

Figure 1 depicts the main tasks performed to determine the validity of new expressions obtained by Plua [21] to predict the behaviour of PATs with variable speeds. The figure comprises three very defined stages: the first shows the activities that are carried out before the numerical simulation, stage two refers to the specific work that is executed during the simulation, and in part three, the post-modelling works are shown, in which the results of the numerical modelling for the analysis case are compared with the experimental data and with the new expressions.
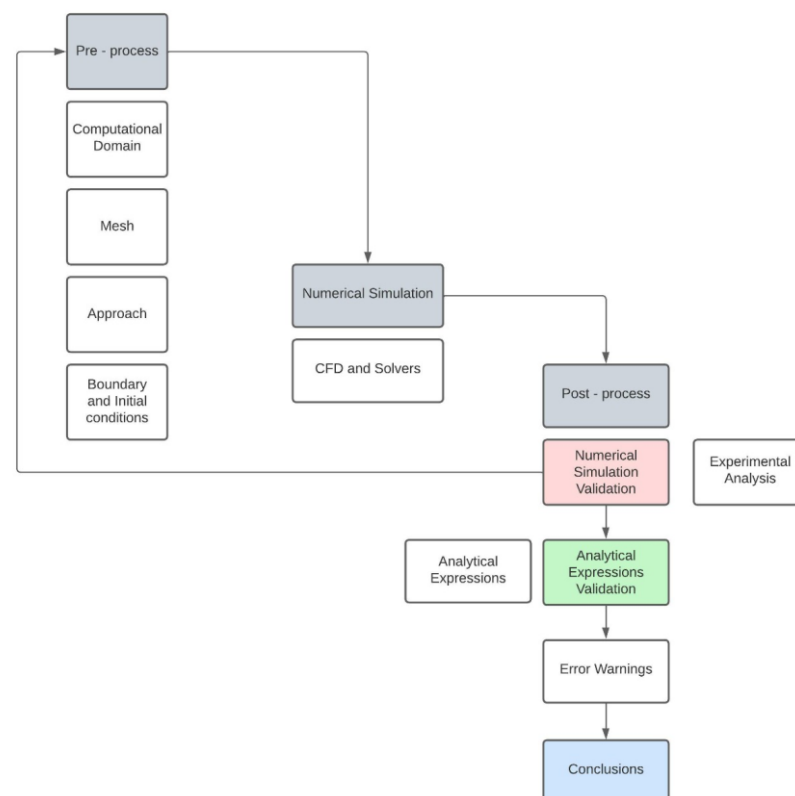
Figure 1. Methodology flowchart.

### 2.1. Preprocess

2.1.1. Computational Domain

The PAT model presented in this study was taken from research conducted by Pérez Sánchez [51] and experimentally tested at the CERIS-Hydraulic Lab of the Instituto Superior of Lisbon, Portugal. The geometry corresponds to an installation of a PAT in

a laboratory that allows experiments where the flow, pressure conditions, and rotational speed can be varied. The hydraulic facility consists of a 1 m³ air vessel tank, a 50 mm HDPE pipe, a KSB radial impeller centrifugal pump (model Etarnom 232) that operates in turbine mode, a regulating tank, pressure transducers, valves, and a flow recirculation pump. The air vessel tank sends water to reach the PAT, which discharges to the open free surface tank and then incorporates it into the system through the recirculation pump. The 3D model was built in the SOLIDWORKS CAD system from which the following drawing view was extracted (see Figure 2). This figure shows the geometry that will be entered into the CFD package and from which the results will be compared with the experimental data and with the new expressions. The interactions of the other elements that comprise the installation of the PAT in the laboratory, such as valves, tank, and pump, are placed in the model through the boundary conditions.

Figure 2. PAT 3D model.

Considering the complexity of this modelling, both due to the geometry and the operation required for the PATs, the computational domain must be divided into parts, which will each be meshed with different meshing levels, with an emphasis on the details of interest and on which of their boundary conditions will be determined individually, to then be configured as a total domain that delivers the results of the whole set. The computational domain consists of four parts: the inlet pipe, starting in the inlet section and reaching the pump's runner; the rotating part that is the impeller of the PAT, the rotating part of the domain; the casing, the stationary part of the pump; and the outlet pipe, which corresponds to the discharge of the pump to the outlet. The original geometry was redefined according to the configuration of the control volumes to obtain the optimal meshing (see Figure 3).
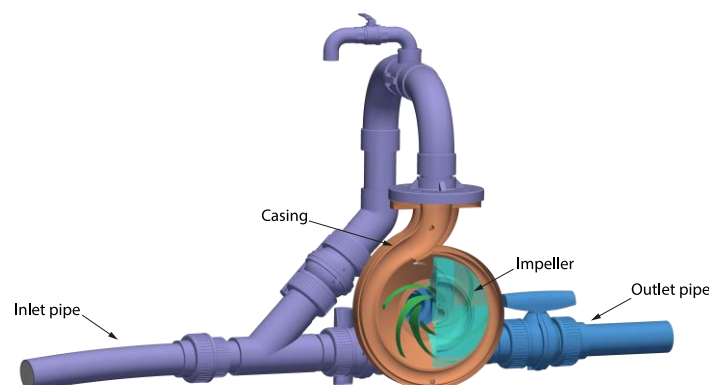
Figure 3. Domains of the case.

Depending on the actual geometry and its characteristics, the .stl files were modified with Autodesk Inventor software (https://www.autodesk.com/products/inventor/overview?term=1-YEAR&tab=subscription) to achieve a better-quality mesh. The areas of meshing interest were prioritised: the casing, the impeller, and the blades. Each has different elements and details with simultaneously different levels and definition angles. It

allows the surfaces to stick more to the edges, bringing the mesh's geometry closer to the actual configuration. The geometries modelled were the volute, the discharge pipe, the inlet pipe, and the impeller. In the case of the impeller, it was divided into three parts, as seen in Figure 3. The impeller is composed of the lower and upper parts and the blades. These elements are treated independently to improve the mesh quality and then facilitate the visualisation of results at the post-processing stage. In addition, six blades were configured inside the impeller, which allowed a better study of the phenomenon presented in the PAT.

2.1.2. Mesh

The mesh was created with snappyHexMesh, an automatic mesh generator that adjusts to the surface to obtain the required mesh. First, the 3D model was exported to format .stl using Autodesk® Inventor® software. Later, with the help of HELIX-OS, the BlockMeshDict file was created to generate, using the BlockMesh utility, orthogonal mesh elements for the casing, inlet pipe, impeller, and outlet, respectively. Once the block meshing was ready, the domain geometries were admitted into the snappyHexMeshDict file. The local refinement was defined using castellatedMesh, and the internal points within the closed domain were entered. Finally, it was necessary to use the topoSet tool to generate zones with movable cells for the runner and merge the meshes with the mergeMeshes utility. The mesh characteristics are presented in Table 2, and the generated mesh is shown in Figure 4. In this figure, the different levels of meshing applied to the subdomains can be seen. In addition, it is observed that their configuration is very close to the original geometry. On the other hand, the model looks appropriately balanced, a situation that is confirmed later.

Table 2. Mesh characteristics.

Parameter	Value/Characteristic
Element type	Hexahedra, Polyhedra, Prism
Number of Elements	827,578
Hexahedral	639,704
Prism	28,238
Polyhedra	159,612
Number of Nodes	1,203,219
Number of Patches	8
Max. Aspect Ratio	14.68619
Min. Surface Area	6.19213^{-9}
Min. Volume	1.39587^{-11}
Max. Skewness	12.918596
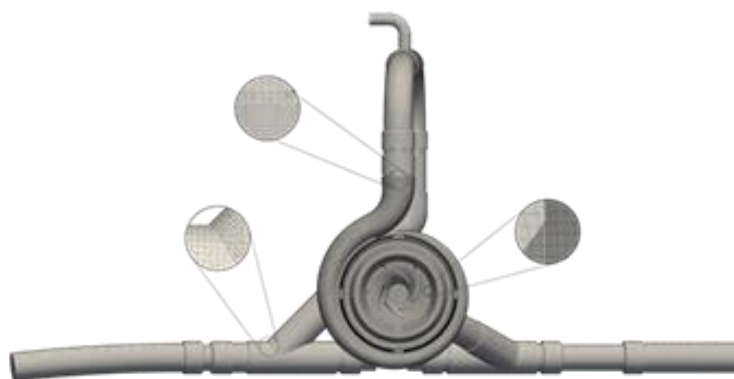
Figure 4. Generated mesh.

2.1.3. Approach

The MRF technique (multiple reference frame) was the technique used for modelling rotation in CFD in this case. This methodology establishes a separate reference frame for each region of the domain, for both rotational and static [49]. It is based on the creation of a local region around the rotating object where the relative velocity is determined for each point. First, Navier–Stokes equations are built, taking into account the centrifugal and Coriolis forces, and then, a set of equations for the stationary and rotational regions are created. This technique can accurately capture instantaneous local flows, which depend on the relative position of the rotative element vs. static geometry. In the MRF approach, the Navier–Stokes equations are solved in terms of the global/inertial velocity. Since, in this case, there is a separation between the impeller and the scroll, the AMI approach is not applicable. For that reason, a set was used that allows a simulation of these elements in the MRF approach.

2.1.4. Boundary and Initial Conditions

Initial and boundary conditions should be applied when solving the Navier–Stokes and continuity equations. Table 3 summarises the initial conditions related to the turbulence models used in this research. For the calibration of the mathematical model, the κ-ε turbulence model was used (the same one used by [51]). κ is turbulent kinetic energy, and ε is turbulent dissipation rate. The κ-ω (specific turbulent dissipation rate)-SST turbulence model was used to analyse the experimental data, the nominal rotational speed curve, and the results of the new expressions contained in [21].

Table 3. Initial conditions.

Initial Conditions	Value
Turbulent Kinetic Energy (κ)	0.032856 (m^2/s^2)
Turbulent Dissipation Rate (ε)	0.320573 (m^2/s^3)
Specific turbulent Dissipation Rate (ω)	108.4104 (s^{-1})
Turbulent kinematic viscosity (nut)	3.03×10^{-4} (m^2/s)

The turbulent kinematic viscosity value "nut" represents the roughness in the walls confirming the domain. Regarding boundary conditions, a constant velocity input condition and a static pressure output condition were used. The boundary conditions of the computational domain are detailed in Table 4.

2.2. Numerical Simulation

2.2.1. CFD

The Navier–Stokes equations were solved using CFD methods based on a continuum mechanics approach for fluid mechanics to define the fluid behaviour in the PATs [50]. For that, two equations were considered that obtain the values of velocity and pressure that allow for defining the average behaviour of the flows. The equations correspond to the conservation of mass and linear momentum and are indicated in a tensor with the following expressions [47]:

$$\frac{\partial \rho}{\partial t} + \overline{u}_j \frac{\partial \rho}{\partial x_j} = 0 \tag{1}$$

$$\frac{\partial(\rho \overline{u}_i)}{\partial t} + \frac{\partial(\rho \overline{u}_i \overline{u}_j)}{\partial x_j} = -\frac{\partial \overline{P}}{\partial x_i} + \frac{\partial\left(\overline{\tau}_{ij} - \tau'_{ij}\right)}{\partial x_j} \tag{2}$$

where *i* and *j* are subscripts for the three axes of space, respectively; $\overline{u}$ is the filtered velocity magnitude; $\overline{P}$ is the filtered pressure; the subgrid stress tensor is $\overline{\tau}_{ij}$; and τ'_{ij} is the filtered viscous stress tensor.

Table 4. Boundary conditions.

	Runner1	Runner	RunnerIn	Volute	Pipe—Inlet	Pipe—Outlet	Inlet	Outlet
Velocity (u-m/s)	movingWallVelocity uniform (0 0 0)	movingWallVelocity uniform (0 0 0)	movingWallVelocity uniform (0 0 0)	fixedValue uniform (0 0 0)	fixedValue uniform (0 0 0)	fixedValue uniform (0 0 0)v	flowRateInletVelocity volumetricFlowRate constant 0.0045	inletOutlet valueuniform (0 0 0)
Static Pressure (p-m²/s²)	zeroGradient	zeroGradient	zeroGradient	zeroGradient	zeroGradient	zeroGradient	zeroGradient	uniform 115,198 (810) 116,694 (930) 112,472 (1050) 112,909 (1170) 115,756 (1275) 110,971 (1500)

2.2.2. CFD and Solvers

The CFD package used is the CFD OpenFOAM 9, which models multiphysics simulations applicable to computational fluid dynamics for incompressible and compressible flows with applications in dynamic mesh management to make rotating reference frames with adaptable mesh refinements as required. OpenFOAM uses a directory structure to solve the cases, where the case is the name of the analysis case; the system sets the numerical control to run time and solver; the constant contains the physical properties, modelling, and mesh information; and 0 has the edge conditions, as well as the beginning to the modelling and time directories that correspond to the solutions and derived cases.

Regarding meshing, OpenFOAM has some mesh utilities, such as BlockMesh, snappyHexMesh, foamyHexMesh, and foamyQuadmesh. OpenFOAM also allows the mesh to be generated with other packages, since mesh conversion utilities are compatible with popular mesh formats (Gmsh, Fluent, Ideas, and Netgen, among others). As stated above, snappyHexMesh generated the mesh. The snappyHexMesh utility is an automatic hybrid mesh that divides, refines, and adjusts to the analysed surface, attaching the mesh with complex details of the geometry [52].

For the calibration of the model, the solver simpleFoam was applied to a steady-state incompressible flow based on the SIMPLE (Semi-Implicit Method for Pressure Linked Equations) algorithm for pressure velocity coupling [53], with applications in turbulent and transient flows in pipes.

3. Results

3.1. Numerical Simulation Validation

3.1.1. Mesh Quality

The checkMesh tool was used to evaluate the mesh quality, giving the mesh stats, the overall number of cells of each type, topology, geometry, and conclusions concerning the mesh. Two parameters were used to verify the quality of the mesh; one of them was Ω, which corresponds to the following expression $\Omega = NE/ND$, where ND is the number of nodes and NE is the number of elements. Ω indicating the homogeneity of the mesh, a good mesh quality will present Ω values close to 1, and values close to 2 have very dispersed meshes. For this case study, the calculated Ω value was 0.69, which is acceptable. The other value was the so-called y^+, which verifies the acceptable range of values for the turbulence model. If this value is less than 1, it is considered that the quality of the mesh is good. In this study, it was found that the average y^+ values in all the simulations of the mesh were less than 1.

3.1.2. Calibration

For the CFD simulation validation, two calibrations were performed concerning the Pérez-Sánchez study [51]. The first concerned the mathematical model made with SOLIDWORKS FloEFD, and the second concerned experimental research. In the Pérez-Sánchez CFD model, the simulated global variables were the head (H), the output hydraulic torque (T), the discharge (Q), and the rotational speed (N). Within the simulations, the absolute static pressure contours were obtained for a flow rate of 4.5 L/s and rotation speeds of 810 rpm, 930 rpm, 1050 rpm, 1170 rpm, 1275 rpm, and 1500 rpm. The results showed that the pressure decreased from upstream to downstream as the fluid flowed within the domains and along the impeller, from the inner to the outer region, as the energy was transmitted to the shaft. On the other hand, it was found that the higher the speed, the lower the pressure value downstream of the impeller.

The results of the simulation performed with OpenFOAM in this study are shown in Figures 5 and 6. As can be seen, the pressure decreased from upstream to downstream, and the lowest pressure value occurred at point D (before the first elbow of the volute outlet) for the maximum speed. A comparison with the original work [51] showed a remarkable similarity between the two. It was observed that, in all cases, the passage of the fluid through the PAT showed a similar behaviour, the pressure difference increased as the speed

in the PAT increased. The error of this simulation concerning the original work varied in ranges from 0.014 to 14.297% at points A, B, C, and F of the model (see Table 5).
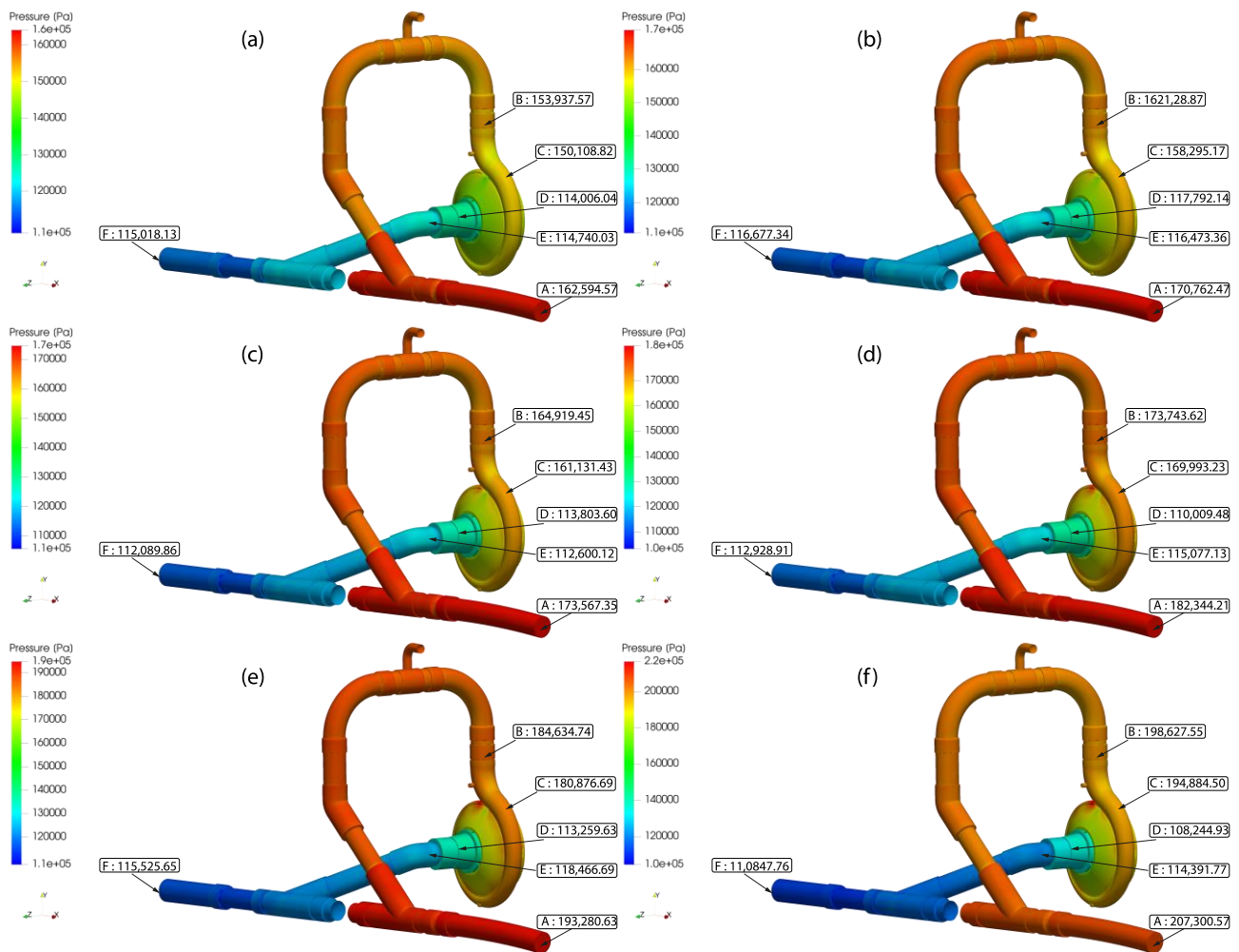
Figure 5. Absolute static pressure contours for Q = 4.50 l/s: (**a**) N = 810 rpm; (**b**) N = 930 rpm; (**c**) N = 1050 rpm; (**d**) N = 1170; (**e**) N = 1275 rpm; (**f**) N = 1500 rpm.

Regarding the calibration of the mathematical simulation with the experimental data, a sensitivity analysis was performed to identify which turbulence model produced the best results. Simulations were executed on the machine's best efficient point (BEP) tested in [51] when operating in turbine mode (Q_{BEP} = 3.6 L/s) for speeds of 200, 600, 880, 1020, 1200, and 1500 rpm using the κ-ε κ-ω-SST models. The results obtained for both simulations are shown in Table 6. As can be seen, the simulations produced errors of similar magnitude. Still, for the nominal rotational speed of 1020 rpm, the κ-ω-SST model was the one with the lowest error. An error index analysis was performed to define the turbulence model with which the cases of experimental data, nominal rotational speed curve, and the results of the new expressions [21] were simulated. Considering that, in all cases, the error indices closest to zero were those that had a better fit and data compatibility, it was observed that the κ-ω-SST turbulence model presented the best fit in all cases. However, it was verified that the order of magnitude of both turbulence models was close, so they proved their validity when they were applied. Figure 7 shows that, in all cases, the κ-ω-SST model had a better performance. Therefore, the κ-ω-SST turbulence model was adopted for the rest of the cases.
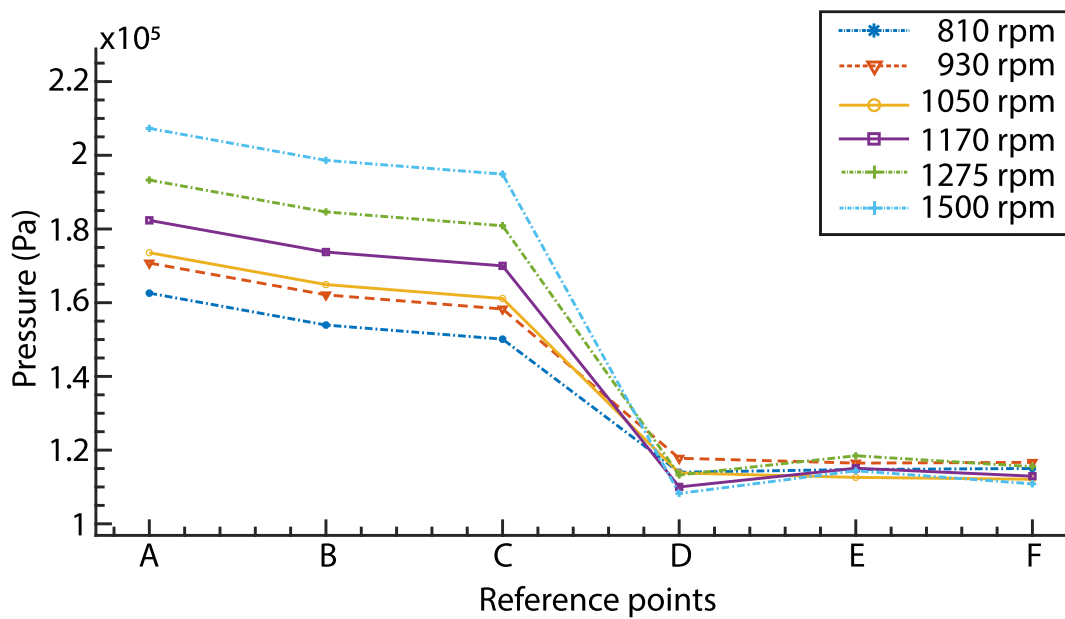
Figure 6. Absolute static pressure vs. referenced sections.

Table 5. Calibration results at points A, B, C, and F compared to [51].

Referenced Sections	% Error					
	810	930	1050	1170	1275	1500
A	8.724%	14.297%	8.218%	0.035%	12.881%	14.042%
B	4.455%	10.425%	4.286%	5.324%	9.068%	13.066%
C	5.979%	12.040%	5.643%	3.999%	10.389%	11.936%
F	0.156%	0.014%	0.340%	0.018%	0.199%	0.111%

Table 6. Sensitivity analysis for κ-ε vs. κ-ω-SST.

	Experimental	Simulation			
		κ-ε		κ-ω-SST	
n (rpm)	H (mca)	H (mca)	% Error	H (mca)	% Error
200	3.27	2.28	30.23	2.39	27.00
600	3.66	2.90	20.74	3.02	17.58
880	4.68	4.21	10.10	4.27	8.73
1020	5.22	5.03	3.67	5.08	2.70
1200	6.22	6.21	0.12	6.14	1.30
1500	7.86	8.60	9.35	8.77	11.52

Once the mathematical model has been validated concerning the results obtained in the numerical modelling and experimental works in [51], the curve of the machine working at nominal speed is contrasted, as seen in Figure 8. In both cases, the increasing trend is shown as a function of the increase in flow rate. In this figure, it is observed that the best results are shown near the volumetric flow value equal to 3.6 L/s, which is precisely the QBEP.
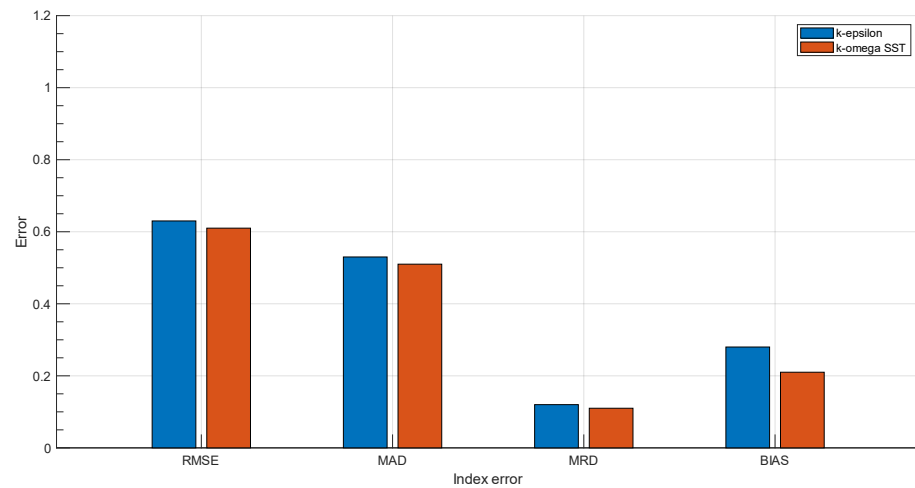
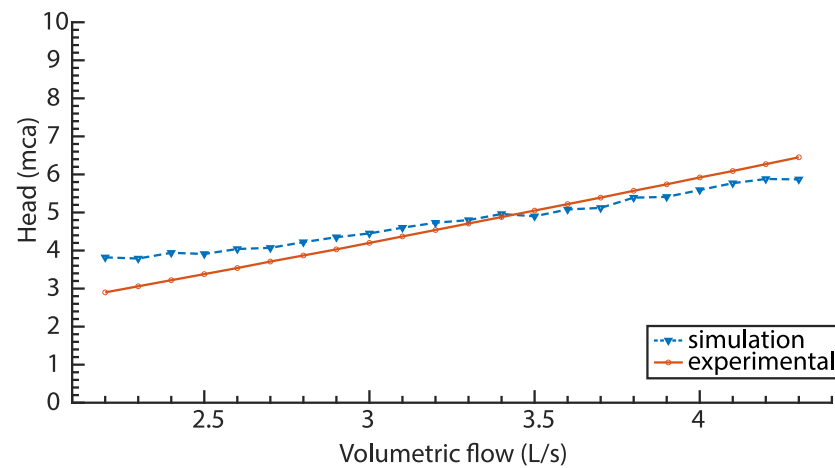**Figure 7.** Index error analysis for the sensitivity analysis.

Figure 8. The nominal curve obtained with CFD OpenFOAM vs. the nominal curve in [51].

The stability of the simulation is related to the convergence, which can be seen in Figure 9, where the residuals of the velocity, pressure, k, and omega are observed. According to this figure, the modelling is considered stable, since all values are less than 10^{-3}.
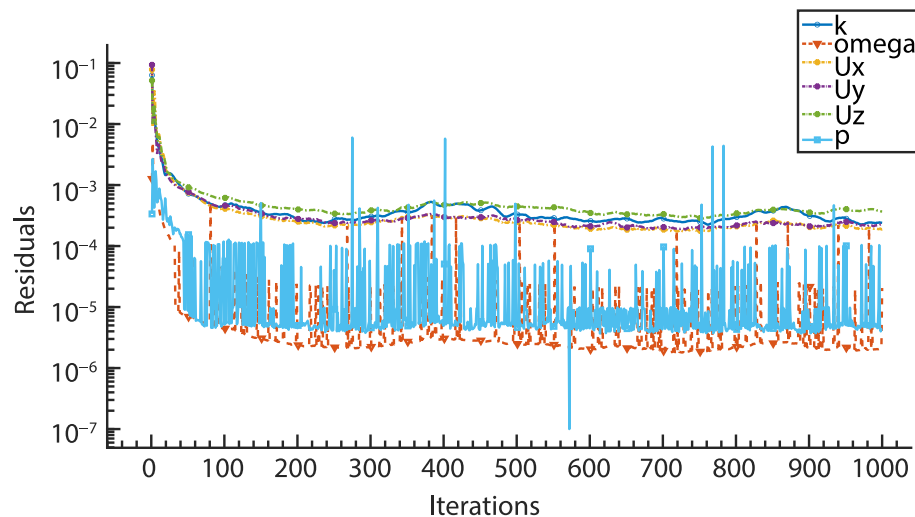

Figure 9. Stability and convergence of the model.

As can be seen, the simulation performed with OpenFOAM presents satisfactory results, and therefore, the model is considered validated. The errors comparing the proposed expressions and the simulations are quite acceptable near the BEP for these sorts of numerical models.

3.2. Analytical Expressions Validation

3.2.1. Analytical Expressions—New Expressions to Predict PATs Behaviour

Considering that, in the case of PATs, the information to select the suitable machines is not known because it is not provided by the manufacturers [54], polynomial expressions have been proposed as a function of semiempirical methods to estimate the characteristic curves in PATs when the rotational speed is constant [20,54–56]. However, considering that flow rates in water systems are variable due to user demand, an optimal energy analysis for PATs cannot be performed if the rotational speed is considered constant. Therefore, strategies have been proposed to maximise energy when the machine works at different rotational speeds, called the variable operation strategy (VOS) [19]. Plua et al. [21] proposed new empirical expressions applying the VOS strategy in water systems for different rotational speeds of 15 different machines and analysing 87 different curves with 56,450 operating points.

Through a mathematical analysis of 10 general expressions (6 polynomials and 4 potentials) considering specific variables as the ratio of rotational speed α and the ratio Q/QBEP, it was possible to adjust a polynomial function for experimental values of head and efficiency and a potential function for power. These expressions are observed in Equations (3)–(7) and present the lowest errors (30 to 50% compared to other models) in the respective analyses performed where the RMSE, MAD, MRD, and BIAS indices were calculated. Equations (3)–(7) correspond to the expressions proposed in [21] to calculate the flow number (q), the head number (h), the efficiency number (e), and the torque number (p), which are dimensionless parameters and correspond to the relationship between the current conditions of the PATs and the best efficient point (BEP) of the machine, to predict the characteristics curves of the PATs when the pump is used in turbine mode. Figure 6 in [21] shows a head and efficiency curve comparison between the proposed model, experimental data, and other models.

$$q = -0.1525 \left(\alpha \frac{Q}{Q_{BEP}} \right) + 0.1958 \left(\frac{Q}{Q_{BEP}} \right)^2 - 0.0118 \left(\frac{Q}{Q_{BEP}} \right) - 0.6429\alpha^2 + 1.8489\alpha - 0.2241 \tag{3}$$

$$h = -0.31070 \left(\alpha \frac{Q}{Q_{BEP}} \right) + 0.3172 \left(\frac{Q}{Q_{BEP}} \right)^2 - 0.0546 \left(\frac{Q}{Q_{BEP}} \right) + 0.242\alpha^2 + 1.1708\alpha - 0.3426 \tag{4}$$

$$e = 0.8271 \left(\alpha \frac{Q}{Q_{BEP}} \right) - 0.3187 \left(\frac{Q}{Q_{BEP}} \right)^2 - 0.1758 \left(\frac{Q}{Q_{BEP}} \right) - 1.035\alpha^2 + 1.1815\alpha + 0.5019 \tag{5}$$

$$p = \alpha^{2.4762} \tag{6}$$

$$q = \alpha^{0.7439} \tag{7}$$

where

$$q = \frac{Q_i}{Q_{BEP}}; h = \frac{H_i}{H_{BEP}}; e = \frac{\eta_i}{\eta_{BEP}}; p = \frac{P_i}{P_{BEP}} = qhe$$

3.2.2. Analytical Expressions Validation

The head value H for different rotational speeds at points close to the BEP was compared with the experimental head obtained in [51], the expressions proposed in [21],

and the mathematical model (see Figure 10). As can be seen, the relationship between Q and H increased in all cases. Figure 11d,e present the best results. It is also observed that the numerical modelling is always closer to reality; the growth slopes are very similar, unlike the other methodology, where this slope is lower. The predictions made in the numerical simulation with OpenFOAM and with the new expressions present values close to the experimental ones when the operation of the machine approaches the BEP.
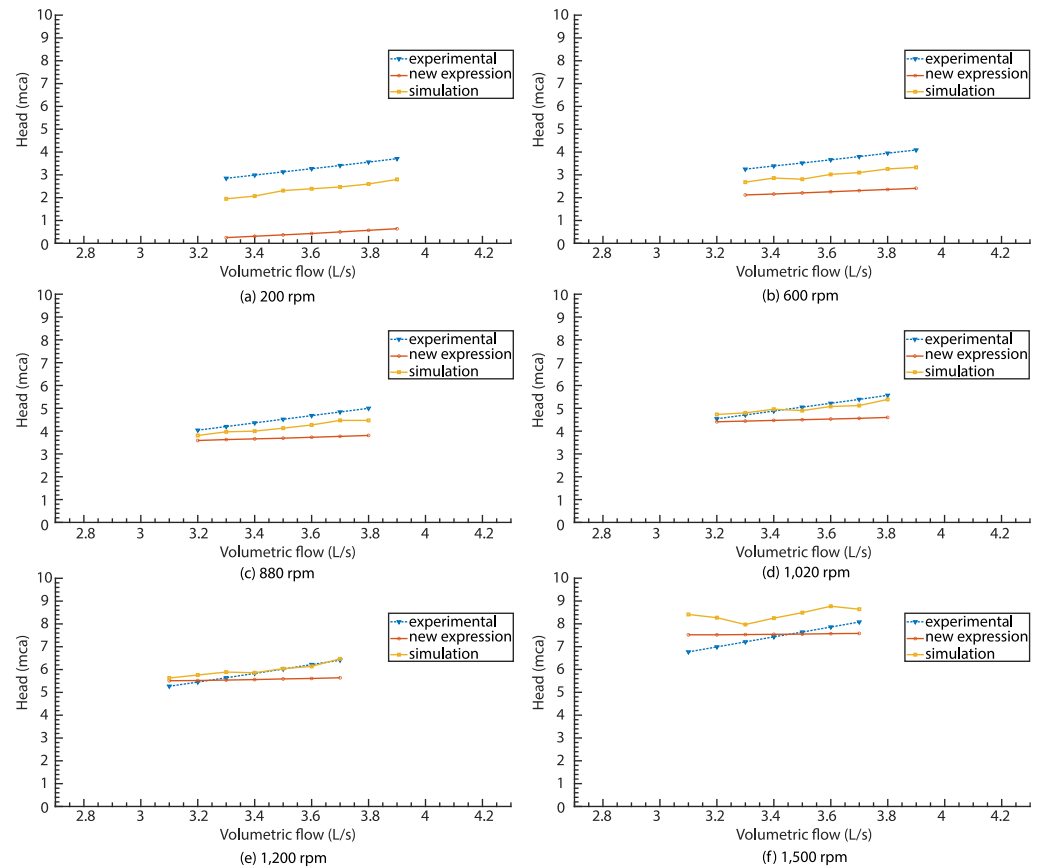

Figure 10. Experimental head [51] vs. head obtained with new expressions in [21] and CFD Open-FOAM simulation.
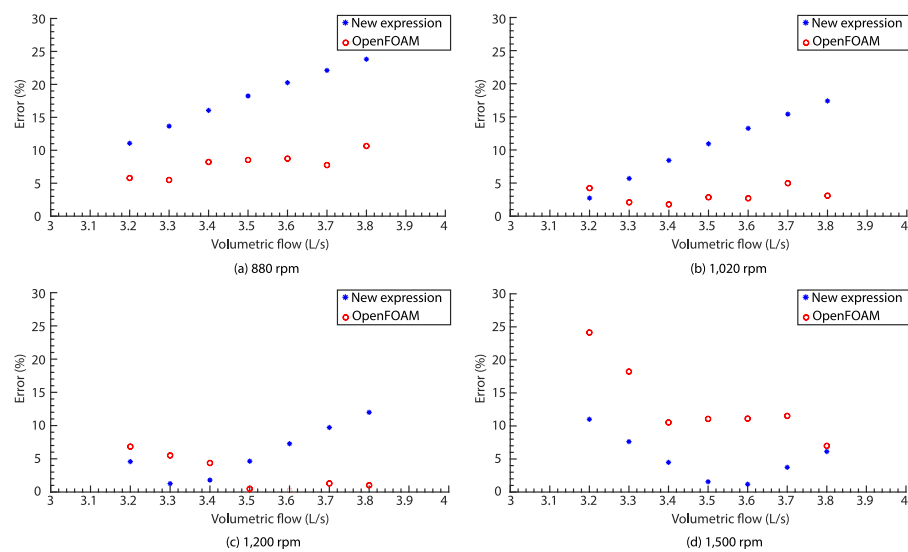

Figure 11. Error correlations.

3.2.3. Error Analysis

The error indices obtained in the predictions made as a function of the rotational speed are presented in Figure 12. As can be seen, as the conditions approach those of the BEP, the predictions reflect values closer to reality. As in other cases, the best results occur when the speed is between 1020 rpm and 1200 rpm. The results of the calculations of the absolute errors are shown in Table 7. In the case of the CFD methodology, the range is from 0 to 11%, while, with the new expressions, this range varies between 1 and 24%.
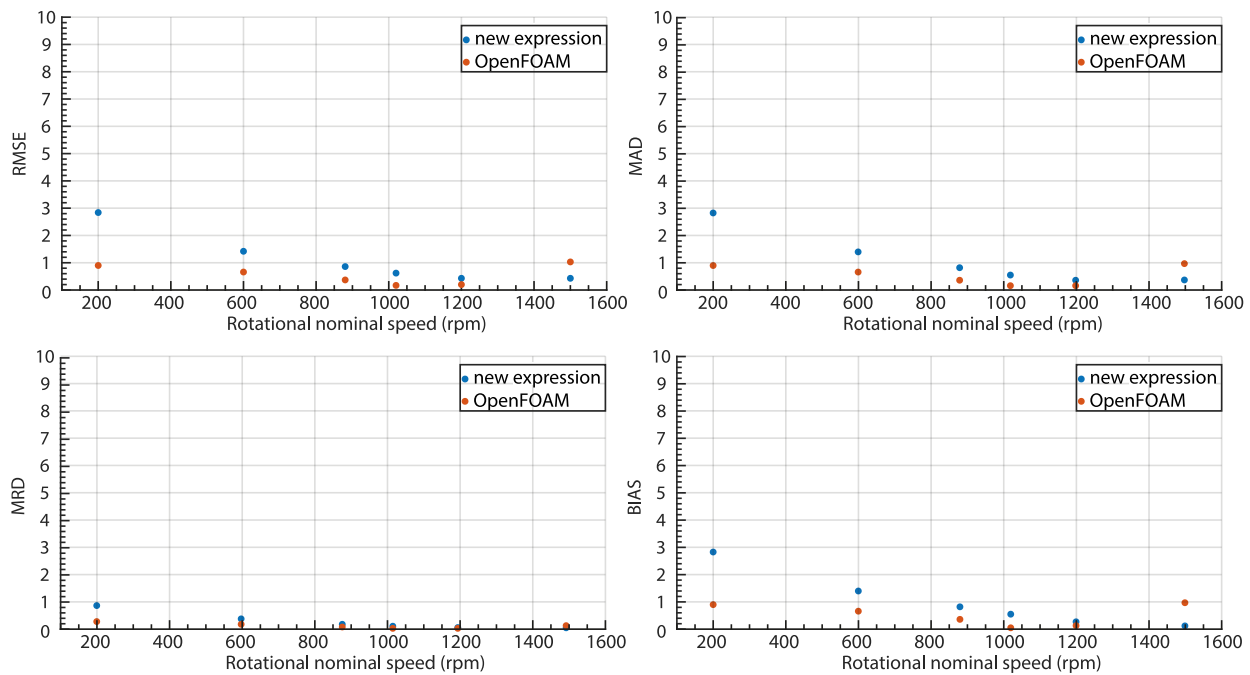

Figure 12. Error indices condidered as RMSE, MAD, MRD and BIAS.

Table 7. Calculated absolute errors.

	Range of Absolute Error			
	OpenFOAM		New Expressions [21]	
n (rpm)	**Min (%)**	**Max (%)**	**Min (%)**	**Max (%)**
880	5	11	11	24
1020	2	5	3	17
1200	0	7	1	12
1500	1	11	7	24

4. Conclusions

This research proposes to validate as a prediction methodology of flow (Q) vs. head (H) curves of variable speed PATs, the numerical simulation with OpenFOAM 3D Free Code Package, depending on its configuration and working conditions. It also proposes to validate the new expressions submitted by Plua [21]. It was demonstrated that the simulation presents adequate results once the mathematical model and the nominal curve of Pérez-Sánchez's [51] research were calibrated. Furthermore, based on experimental data from a PAT, the Q vs. H curves were calculated through the new expressions [21], as well as with the numerical simulation performed in OpenFOAM, presenting satisfactory results as the operation point of the work approached the BEP, since the trend of the generated curves, the slope thereof, and the error indices demonstrated acceptable values. However, when moving away from the BEP conditions, the error increased.

In summary, it was possible to validate the prediction methodologies of the Q vs. H characteristic curves of the PATs and verify the range in which they present the best results. This study can be extended through the tuning of the coefficients of the proposed analytical expressions based on the feedback with new experimental data.

Author Contributions: Conceptualisation, M.P.-S. and P.A.L.-J.; methodology, F.A.P., F.-J.S.-R., and M.P.-S. software, writing—original draft preparation, V.H., F.A.P., and M.P.-S.; writing—review and editing, P.A.L.-J. and M.P.-S.; visualisation M.P.-S. and P.A.L.-J.; and supervision, M.P.-S. and P.A.L.-J. All authors have read and agreed to the published version of the manuscript.

Institutional Review Board Statement: Not applicable.

Informed Consent Statement: Not applicable.

Data Availability Statement: Not applicable.

Conflicts of Interest: The authors declare no conflict of interest.

References

1. Farley, M. *Leakage Management and Control*; WHO: Geneva, Switzerland, 2001; pp. 1–98. Available online: http://whqlibdoc.who.int/hq/2001/WHO_SDE_WSH_01.1_pp1-98.pdf (accessed on 1 May 2023).
2. Niu, W.-J.; Feng, Z.-K. Evaluating the performances of several artificial intelligence methods in forecasting daily streamflow time series for sustainable water resources management. *Sustain. Cities Soc.* **2020**, *64*, 102562. [CrossRef]
3. Ebrahimi, S.; Riasi, A.; Kandi, A. Selection optimization of variable speed pump as turbine (PAT) for energy recovery and pressure management. *Energy Convers. Manag.* **2020**, *227*, 113586. [CrossRef]
4. Orouji, H.; Haddad, O.B.; Fallah-Mehdipour, E.; Mariño, M.A. Modeling of Water Quality Parameters Using Data-Driven Models. *J. Environ. Eng.* **2013**, *139*, 947–957. [CrossRef]
5. Vakilifard, N.; Anda, M.; Bahri, P.A.; Ho, G. The role of water-energy nexus in optimising water supply systems—Review of techniques and approaches. *Renew. Sustain. Energy Rev.* **2018**, *82*, 1424–1432. [CrossRef]
6. Ferrarese, G.; Malavasi, S. Perspectives of Water Distribution Networks with the GreenValve System. *Water* **2020**, *12*, 1579. [CrossRef]
7. Islam, M.S.; Babel, M.S. Economic Analysis of Leakage in the Bangkok Water Distribution System. *J. Water Resour. Plan. Manag.* **2013**, *139*, 209–216. [CrossRef]
8. Bibri, S.E.; Krogstie, J. Smart sustainable cities of the future: An extensive interdisciplinary literature review. *Sustain. Cities Soc.* **2017**, *31*, 183–212. [CrossRef]
9. Bach, P.M.; Rauch, W.; Mikkelsen, P.S.; McCarthy, D.T.; Deletic, A. A critical review of integrated urban water modelling—Urban drainage and beyond. *Environ. Model. Softw.* **2014**, *54*, 88–107. [CrossRef]
10. Raboaca, M.S.; Bizon, N.; Trufin, C.; Enescu, F.M. Efficient and Secure Strategy for Energy Systems of Interconnected Farmers' Associations to Meet Variable Energy Demand. *Mathematics* **2020**, *8*, 2182. [CrossRef]
11. Morani, M.C.; Carravetta, A.; D'ambrosio, C.; Fecarotta, O. A New Preliminary Model to Optimize PATs Location in a Water Distribution Network. *Environ. Sci. Proc.* **2020**, *2*, 57. [CrossRef]
12. Gupta, A.; Bokde, N.; Marathe, D.; Kulat, K. Leakage Reduction in Water Distribution Systems with Efficient Placement and Control of Pressure Reducing Valves Using Soft Computing Techniques. *Eng. Technol. Appl. Sci. Res.* **2017**, *7*, 1528–1534. [CrossRef]
13. Ávila, C.A.M.; Sánchez-Romero, F.J.; López-Jiménez, P.A.; Pérez-Sánchez, M. Improve leakage management to reach sustainable water supply networks through by green energy systems. Optimized case study. *Sustain. Cities Soc.* **2022**, *83*, 103994. [CrossRef]
14. Ramos, H.M.; Borga, A. Pumps as turbines: An unconventional solution to energy production. *Urban Water* **1999**, *1*, 261–263. [CrossRef]
15. Gallagher, J.; Harris, I.M.; Packwood, A.J.; McNabola, A.; Williams, A.P. A strategic assessment of micro-hydropower in the UK and Irish water industry: Identifying technical and economic constraints. *Renew. Energy* **2015**, *81*, 808–815. [CrossRef]
16. Ávila, C.A.M.; Sánchez-Romero, F.-J.; López-Jiménez, P.A.; Pérez-Sánchez, M. Leakage Management and Pipe System Efficiency. Its Influence in the Improvement of the Efficiency Indexes. *Water* **2021**, *13*, 1909. [CrossRef]
17. Ávila, C.A.M.; Sánchez-Romero, F.-J.; López-Jiménez, P.A.; Pérez-Sánchez, M. Definition of the Operational Curves by Modification of the Affinity Laws to Improve the Simulation of PATs. *Water* **2021**, *13*, 1880. [CrossRef]
18. Ávila, C.A.M.; Sánchez-Romero, F.-J.; López-Jiménez, P.A.; Pérez-Sánchez, M. Optimization tool to improve the management of the leakages and recovered energy in irrigation water systems. *Agric. Water Manag.* **2021**, *258*, 107223. [CrossRef]
19. García, I.F.; Novara, D.; Mc Nabola, A. A Model for Selecting the Most Cost-Effective Pressure Control Device for More Sustainable Water Supply Networks. *Water* **2019**, *11*, 1297. [CrossRef]

20. Pérez-Sánchez, M.; Sánchez-Romero, F.J.; Ramos, H.M.; López-Jiménez, P.A. Improved Planning of Energy Recovery in Water Systems Using a New Analytic Approach to PAT Performance Curves. *Water* **2020**, *12*, 468. [CrossRef]

21. Plua, A.F.; Sánchez-Romero, F.-J.; Hidalgo, V.; López-Jiménez, P.A.; Pérez-Sánchez, M. New Expressions to Apply the Variation Operation Strategy in Engineering Tools Using Pumps Working as Turbines. *Mathematics* **2021**, *9*, 860. [CrossRef]

22. Lee, S.; Pomeroy, C.; Burian, S. Setting Future Water Rates for Sustainability of a Water Distribution System. *J. Water Resour. Plan. Manag.* **2021**, *147*, 04020108. [CrossRef]

23. Ahmadi, S.; Saboohi, Y.; Vakili, A. Frameworks, quantitative indicators, characters, and modeling approaches to analysis of energy system resilience: A review. *Renew. Sustain. Energy Rev.* **2021**, *144*, 110988. [CrossRef]

24. Stefanizzi, M.; Capurso, T.; Balacco, G.; Binetti, M.; Camporeale, S.M.; Torresi, M. Selection, control and techno-economic feasibility of Pumps as Turbines in Water Distribution Networks. *Renew. Energy* **2020**, *162*, 1292–1306. [CrossRef]

25. Renzi, M.; Rudolf, P.; Štefan, D.; Nigro, A.; Rossi, M. Installation of an axial Pump-as-Turbine (PaT) in a wastewater sewer of an oil refinery: A case study. *Appl. Energy* **2019**, *250*, 665–676. [CrossRef]

26. Sánchez, M.P.; Sánchez-Romero, F.J.; Ramos, M.H.; López-Jiménez, P.A. *Bombas Operando Como Turbinas (PAT): Principios de Funcionamiento y Selección*; Universidad Politécnica de Valencia: Valencia, Spain, 2020.

27. Binama, M.; Su, W.-T.; Li, X.-B.; Li, F.-C.; Wei, X.-Z.; An, S. Investigation on pump as turbine (PAT) technical aspects for micro hydropower schemes: A state-of-the-art review. *Renew. Sustain. Energy Rev.* **2017**, *79*, 148–179. [CrossRef]

28. Novara, D.; Carravetta, A.; McNabola, A.; Ramos, H.M. Cost Model for Pumps as Turbines in Run-of-River and In-Pipe Microhydropower Applications. *J. Water Resour. Plan. Manag.* **2019**, *145*, 04019012. [CrossRef]

29. Thoma, D.; Kittredge, C.P. Centrifugal pumps operated under abnormal conditions. *J. Power Sources* **1931**, *73*, 881–884.

30. Stepanoff, A.J. *Centrifugal and Axial Flow Pumps: Theory, Design, And Application*; Krieger Publishing Company: Malabar, FL, USA, 1957.

31. Childs, S. Convert pumps to turbines and recover HP. *Hydrocarb. Process. Pet. Refin.* **1962**, *41*, 173–174.

32. Jain, S.V.; Patel, R.N. Investigations on pump running in turbine mode: A review of the state-of-the-art. *Renew. Sustain. Energy Rev.* **2014**, *30*, 841–868. [CrossRef]

33. Fecarotta, O.; McNabola, A. Optimal Location of Pump as Turbines (PATs) in Water Distribution Networks to Recover Energy and Reduce Leakage. *Water Resour. Manag.* **2017**, *31*, 5043–5059. [CrossRef]

34. Moazeni, F.; Khazaei, J. Optimal energy management of water-energy networks via optimal placement of pumps-as-turbines and demand response through water storage tanks. *Appl. Energy* **2021**, *283*, 116335. [CrossRef]

35. Rossi, M.; Renzi, M. A general methodology for performance prediction of pumps-as-turbines using Artificial Neural Networks. *Renew. Energy* **2018**, *128*, 265–274. [CrossRef]

36. Prasad, V.; Shukla, S.N.; Joshi, S.G. Performance characteristics of pump as turbine. *Indian Pumps* **2006**, *38*, 5–9.

37. Williams, A. Pumps as turbines for low cost micro hydro power. *Renew. Energy* **1996**, *9*, 1227–1234. [CrossRef]

38. Páscoa, J.C.; Silva, F.J.; Pinheiro, J.S.; Martins, D.J. A new approach for predicting PAT-pumps operating point from direct pumping mode characteristics. *J. Sci. Ind. Res.* **2012**, *71*, 144–148.

39. Rossi, M.; Righetti, M.; Renzi, M. Pump-as-turbine for Energy Recovery Applications: The Case Study of An Aqueduct. *Energy Procedia* **2016**, *101*, 1207–1214. [CrossRef]

40. Plua, F.; Hidalgo, V.; Cando, E.; Pérez-Sánchez, M.; López-Jiménez, P. Pumps as Turbines (PATs) by Analysis with CFD Models. *Int. J. Adv. Sci. Eng. Inf. Technol.* **2022**, *12*, 1098–1104. [CrossRef]

41. Rawal, S.; Kshirsagar, J.T. Numerical Simulation on a Pump Operating in a turbine mode. In Proceedings of the 23rd International Pump Users Symposium, Houston, TX, USA, 5–8 March 2007.

42. Nautiyal, H.; Kumar, A. Reverse running pumps analytical, experimental and computational study: A review. *Renew. Sustain. Energy Rev.* **2010**, *14*, 2059–2067. [CrossRef]

43. Páscoa, J.; Silva, F.J.; Pinheiro, J.S.; Martins, D.J. Accuracy details in realistic CFD modeling of an industrial centrifugal pump in direct and reverse modes. *J. Therm. Sci.* **2010**, *19*, 491–499. [CrossRef]

44. Carravetta, A.; Fecarotta, O.; Ramos, H. Numerical simulation on Pump As Turbine: Mesh reliability and performance concerns. In Proceedings of the 2011 International Conference on Clean Electrical Power (ICCEP), Ischia, Italy, 14–16 June 2011; pp. 169–174.

45. Carravetta, A.; Fecarotta, O.; Del Giudice, G.; Ramos, H. Energy Recovery in Water Systems by PATs: A Comparisons among the Different Installation Schemes. *Procedia Eng.* **2014**, *70*, 275–284. [CrossRef]

46. Pugliese, F.; De Paola, F.; Fontana, N.; Giugni, M.; Marini, G.; Francos, J.F. Experimental and numerical investigation of centrifugal Pumps As Turbines. In Proceedings of the 10th International Conference on Energy Efficiency in Motor Driven System, Rome, Italy, 6–8 September 2017; pp. 6–7.

47. Plua, F.; Hidalgo, V.; López-Jiménez, P.A.; Pérez-Sánchez, M. Analysis of Applicability of CFD Numerical Studies Applied to Problem When Pump Working as Turbine. *Water* **2021**, *13*, 2134. [CrossRef]

48. Nautiyal, H.; Kumar, V.; Thakur, A. CFD Analysis on Pumps Working as Turbines. *Hydro Nepal J. Water Energy Environ.* **2011**, *6*, 35–37. [CrossRef]

49. Hidalgo, V.; Velasco, M.; Cando, E.; Valencia, E.; Simbaña, S.; Puga, D.; Mora, C.; Escaler, X. Rotatory 3D structured mesh study using openFOAM to simulate the flow in francis turbine. *Mater. Today Proc.* **2021**, *49*, 142–148. [CrossRef]

50. Hidalgo, V.; Escaler, X.; Valencia, E.; Peng, X.; Erazo, J.; Puga, D.; Luo, X. Scale-Adaptive Simulation of Unsteady Cavitation Around a Naca66 Hydrofoil. *Appl. Sci.* **2019**, *9*, 3696. [CrossRef]

51. Pérez-Sánchez, M.; Simão, M.; López-Jiménez, P.A.; Ramos, H.M. CFD Analyses and Experiments in a PAT Modeling: Pressure Variation and System Efficiency. *Fluids* **2017**, *2*, 51. [CrossRef]
52. Hidalgo, V.; Díaz, C.; Erazo, J.; Simbaña, S.; Márquez, D.; Puga, D.; Velasco, R.; Mafla, C.; Barragán, G.; Parra, C.; et al. Simplified simulation of a small Pelton turbine using OpenFOAM. *IOP Conf. Ser. Earth Environ. Sci.* **2021**, *774*, 012075. [CrossRef]
53. Huang, S.; Wei, Y.; Guo, C.; Kang, W. Numerical Simulation and Performance Prediction of Centrifugal Pump's Full Flow Field Based on OpenFOAM. *Processes* **2019**, *7*, 605. [CrossRef]
54. Fecarotta, O.; Aricò, C.; Carravetta, A.; Martino, R.; Ramos, H.M. Hydropower Potential in Water Distribution Networks: Pressure Control by PATs. *Water Resour. Manag.* **2014**, *29*, 699–714. [CrossRef]
55. Novara, D.; McNabola, A. A model for the extrapolation of the characteristic curves of Pumps as Turbines from a datum Best Efficiency Point. *Energy Convers. Manag.* **2018**, *174*, 1–7. [CrossRef]
56. Shah, S.R.; Jain, S.V.; Patel, R.N.; Lakhera, V.J. CFD for centrifugal pumps: A review of the state-of-the-art. *Procedia Eng.* **2013**, *51*, 715–720. [CrossRef]